Control of post-disruption runaway electron beams in DIII-D[a)]

N. W. Eidietis,[1,b)] N. Commaux,[2] E. M. Hollmann,[3] D. A. Humphreys,[1] T. C. Jernigan,[2] R. A. Moyer,[3] E. J. Strait,[1] M. A. VanZeeland,[1] J. C. Wesley,[1] and J. H. Yu[3]
[1]*General Atomics, P.O. Box 85608, San Diego, California 92186-5608, USA*
[2]*Oak Ridge National Laboratory, Oak Ridge, Tennessee 37831, USA*
[3]*University of California-San Diego, La Jolla, California 92093-0417, USA*

(Received 16 December 2011; accepted 29 December 2011; published online 28 March 2012)

Recent experiments in the DIII-D tokamak have demonstrated real-time control and dissipation of post-disruption runaway electron (RE) beams. In the event that disruption avoidance, control, and mitigation schemes fail to avoid or suppress RE generation, active control of the RE beam may be an important line of defense to prevent the rapid, localized deposition of RE beam energy onto vulnerable vessel sections. During and immediately after the current quench, excessive radial compression of the runaway beams is avoided by a combination of techniques, improving the likelihood of the beams surviving this dynamic period without a fast termination. Once stabilized, the runaway beams are held in a steady state (out to the ohmic flux limit) with the application of active plasma current and position controls. Beam interaction with the vessel wall is minimized by avoiding distinct thresholds for enhanced wall interaction at small and large radii, corresponding to inner wall and outer limiter interaction, respectively. Staying within the "safe zone" between those radial thresholds allows for the sustainment of long-lived, quiescent runaway beams. The total beam energy and runaway electron population are then dissipated gradually by a controlled ramp-down of the runaway current. © *2012 American Institute of Physics*. [http://dx.doi.org/10.1063/1.3695000]

I. INTRODUCTION

Recent experiments in the DIII-D[1] tokamak have demonstrated active control of relativistic "runaway" electron (RE) beam position and current following a disruption. The purpose of establishing this control is to maintain the runaway beam at a safe position within the vacuum vessel while gradually dissipating its total energy, thereby reducing the potential threat that the beam poses to the in-vessel components of the tokamak.

The rapid change in magnetic flux during a tokamak disruption[2] induces large toroidal electric fields that can accelerate initially thermal electrons to relativistic energies.[3–5] Those relativistic electrons possess a very small collision cross-section[6] and are referred to as "runaway" electrons. The high energy (on the order of a few tens of MeV) of these electrons allows them to penetrate far into the first wall of the tokamak, enabling significant localized power deposition below the protective outer surface.[7]

During the current quench portion of a disruption, the initially small runaway electron population experiences an avalanche multiplication.[8] This can result in a significant portion of the initially thermal plasma current being replaced by runaway electron current. The avalanche gain is an exponential function of the initial plasma current before the current quench, so a high-current tokamak such as ITER,[9] operating with up to 15 MA of plasma current, will possess a gain many orders of magnitude greater than existing devices.[10] This high gain makes ITER particularly susceptible to producing large runaway current fractions (exceeding 10 MA[10]) during a disruption. Given the high likelihood of substantial runaway electron current generation in ITER, as well as the high cost of repairing in-vessel components in an activated nuclear environment, it is important to develop techniques to benignly dissipate runway beam energy, alleviating the threat posed to in-vessel components.

The evolution of post-disruption runaway electron beams has been documented in multiple devices, including JET,[11–15] JT-60U,[16–18] TEXTOR,[15] and Tore Supra.[19–22] This paper expands upon those reports, describing in detail the integrated methodology used to catch, hold, and safely dissipate runaway electron beams in DIII-D. Section II describes the production and diagnosis of these beams in DIII-D. This is followed by the techniques developed to stabilize the position of a runaway beam during and immediately after the current quench in Sec. III. Section IV describes slow timescale control of runaway beams during the "plateau" phase. Section V presents the radial thresholds that determine a "safe" position for holding the runaway beam with minimal wall interaction. Finally, Sec. VI details the gradual, controlled dissipation of the runaway beam current and energy.

II. RUNAWAY ELECTRON PRODUCTION AND DIAGNOSTICS

Runaway electron beams are very rarely observed during naturally occurring disruptions in DIII-D. This may be due to a combination of low I_p (~1.5 MA) leading to low runaway electron avalanche gain (~50-100), a marginal toroidal field strength (2.1 T) for runaway electron production,[13,23] and seed runaway loss along stochastic field lines following the thermal quench.[24] The most reliable means for

[a)]Paper VI3 1, Bull. Am. Phys. Soc. **56**, 355 (2011).
[b)]Invited speaker. Electronic mail: eidietis@fusion.gat.com.

producing runaway electron beams in DIII-D is to inject a small cryogenic argon pellet (8 Torr-L) into the plasma, forcing the onset of the thermal and current quenches.[25] All runaway beams described in this paper were produced in this manner.

The shape of the target plasma into which the pellet is fired has a significant impact upon the reliability of runaway electron production from discharge to discharge. Low elongation ($\kappa = 1.2 - 1.5$) inner wall limited (IWL) targets are observed to yield runaway electron plateaus much more regularly than more elongated, diverted target configurations. This phenomenon has also been reported in JET.[13] 3D resistive MHD simulations suggest that this shape dependence is a function of the degree of magnetic island overlap and the resulting field stochasticity during the thermal quench.[24] In DIII-D, lower single null targets typically yield observable runaway electron plateaus in less than 15% of discharges, whereas inner wall limited targets can produce runaway plateaus with greater than 50% reliability on a given run day. All runaway beams described in this paper originated from low elongation IWL targets. This magnetic configuration is vertically stable, so minimal active stabilization of the runaway beam vertical position during and immediately after the current quench is necessary.

The target plasmas are in L-mode, heated by 1-3 MW of electron cyclotron heating (ECH) power. Typical parameters immediately preceding the arrival of the argon pellet are $I_p = 1.2 - 1.5$ MA, line averaged density $n_e = 2 - 3 \times 10^{19}$ m^{-3}, and central electron temperature $T_e = 1.5 - 3$ keV.

Several diagnostics are available to observe the evolution of runaway beams on DIII-D. A fast framing camera, equipped with a narrow band-pass filter to eliminate line radiation, provides a wide-view, 2D image of the visible synchrotron emission from the runaway beam.[26] Plastic and ZnS scintillation detectors[27] provide single-point measurements of the hard x-rays (HXRs) and photo-neutrons emitted by runaway electron collisions with the vessel wall or plasma ions. In addition, a toroidally and poloidally distributed array of 12 barium germanium oxide (BGO) HXR/gamma scintillators allows spatial resolution of the runaway beam emission.[28]

The timeline for a typical DIII-D runaway electron beam is shown in Fig. 1. The argon pellet is fired at 2.0 s. The pellet ablates as it crosses the plasma boundary, producing a flash of visible light, shown in Fig. 1(a). The argon immediately causes rapid thermal quench, as evidenced by the sudden drop in electron temperature shown in Fig. 1(b). Within a few milliseconds, the now-cold plasma undergoes a current quench, as noted in Fig. 1(c). The high loop voltage induced by the rapid drop in current results in the thermal plasma current [indicated by the dashed line in Fig. 1(c)], being replaced by a rapidly increasing runaway electron current, creating a runaway electron "plateau." The HXR signal [Fig. 1(d)] exhibits an early "prompt loss" spike during the current quench, indicating fast deconfinement of the initial seed runaway electrons to the wall. As the runaway electron current matures into a plateau, the HXR signal grows and eventually plateaus as well. A final large HXR spike coincident with a rapid termination in the runaway current (I_{RE}) indicates the complete deconfinement of the remaining runaway electrons to the wall.

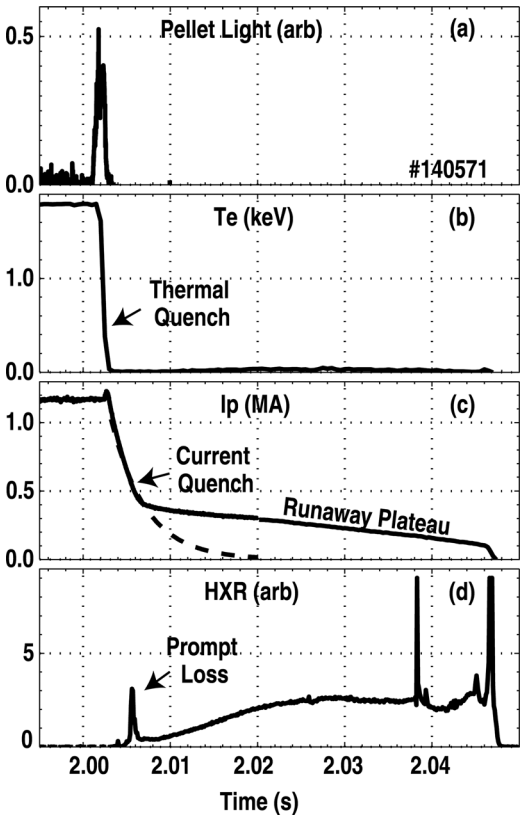

FIG. 1. Typical evolution of an uncontrolled runaway electron beam in DIII-D. Argon pellet is launched at 2.0 s. The dashed line in (c) indicates an exponential fit to the initial L/R decay of the thermal plasma, extrapolated into the runaway plateau.

III. CONTROL DURING THE CURRENT QUENCH

During and immediately following the current quench, the changes in force balance work to radially compress of the original target plasma shape onto the inner wall. This results in a much smaller runaway beam at the end of the current quench, as illustrated by the light and dark plasma boundaries in Fig. 2.

There are two primary contributors to this compression. First, the outer poloidal field (PF) coils (noted in Fig. 2) that provide the bulk of the vertical field (B_z) required for maintaining radial equilibrium cannot slew fast enough to compensate fully for either the drop in plasma pressure during the thermal quench or the subsequent rapid drop in I_p experienced during the current quench. The mismatched B_z results in the plasma being pushed into the inner wall. During DIII-D shots producing runaway electron beams, an 80% drop in I_p (1.5 to 0.3 MA) over a 5 ms current quench is typical. Fortunately, the large voltages that the current quench induces in the outer poloidal field coils drive those coils' currents toward zero, partially compensating for the inadequate power supply voltage and reducing the degree of radial compression. However, the current quench also induces attractive currents in the inner PF coils, annotated in Fig. 2, as well as the inboard vessel wall. Those currents are the second

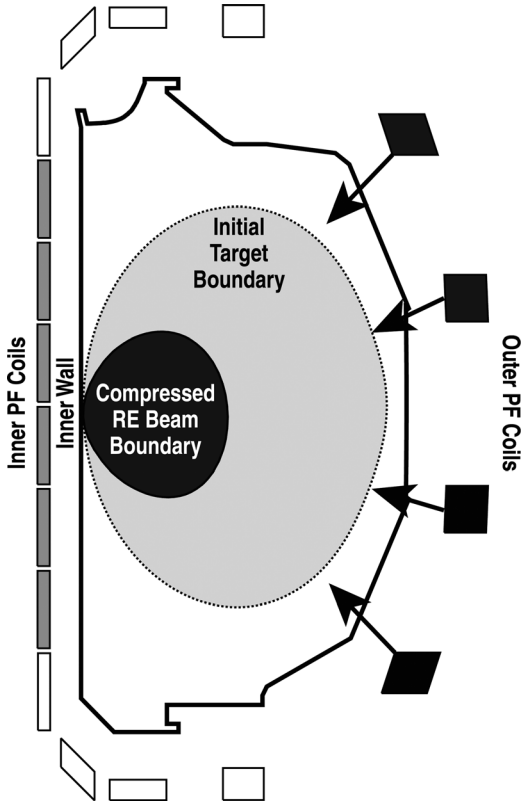

FIG. 2. Compression of runaway beam boundary occurring during the current quench. The light "target boundary" indicates the target plasma shape prior to the arrival of the argon pellet. The black "RE beam boundary" is the runaway beam boundary after the current quench.

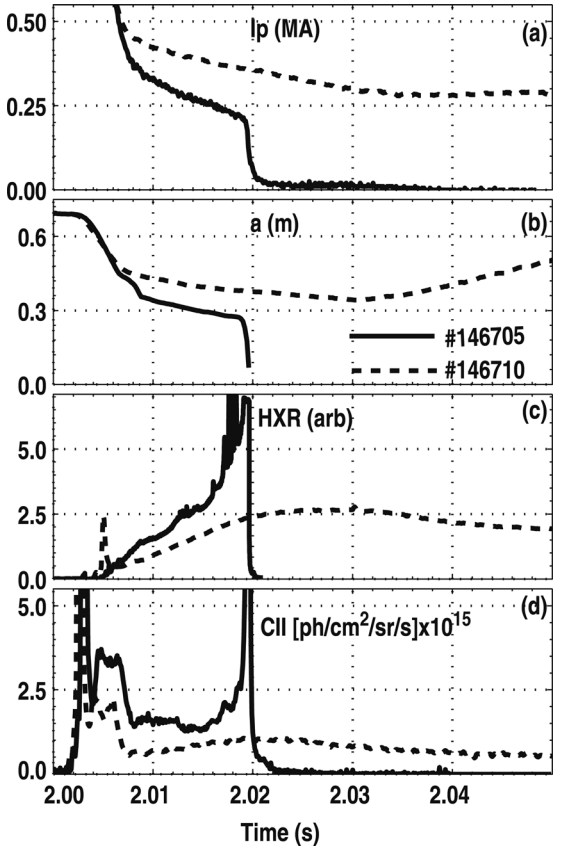

FIG. 3. Effects of excessive radial compression during and after the current quench. Solid line indicates a highly compressed, short lived runaway beam. Dotted line indicates a long-lived runaway beam for comparison.

contributing factor to the radial compression of the runaway beam, as they serve to pull the beam into the inner wall.

Excessive radial compression leads to rapid termination of the runaway beam. This phenomenon is illustrated in Fig. 3. Fig. 3(a) displays the I_p traces of two discharges transitioning from the current quench into the runaway plateau phase. One runaway beam (solid line) terminates rapidly less than 15 ms after the end of the current quench, whereas the other beam (dashed line) survives for a much longer time. The short-lived runaway electron beam possesses lower initial runaway current, so it compresses faster and farther than the long-lived case, as shown by the trace of minor radius (a) in Fig. 3(b). Once the minor radius reaches approximately 0.3 m, the HXR emission of the short-lived beam quickly rises far above that of the long-lived beam [Fig. 3(c)]. This rapid rise in HXR signal is indicative of increasing runaway electron deconfinement to the wall. At the same time, the carbon light also peaks, indicating enhanced runaway electron interaction with the carbon tiles of the first wall [Fig. 3(d)]. The increasing impurity content further increases the drag on the runaway beam, increasing the current damping rate. This activity is soon followed by a termination of the short-lived runaway beam at 2.02 s.

A basic control scheme has been developed in DIII-D to reduce the degree of runaway electron beam radial compression following the current quench. This method cannot guarantee the survival of every runaway beam (particularly those with excessively low initial runaway current), but it does significantly improve the likelihood of a long-lived runaway plateau.

The first step is to apply an open-loop, saturated voltage command to the inner poloidal field coils during and immediately following the current quench. While this applied voltage cannot prevent the current quench inducing attractive currents in the coils, it does remove those currents on a much faster time-scale (20-30 ms) than the uncompensated L/R decay of the coils (80 ms), as shown in Fig. 4(a).

At the same time, a positive loop voltage is applied with the ohmic solenoid in order to promote increased runaway current, also reducing radial compression. This loop voltage causes little change during the current quench, but it can provide aid in the less dynamic period immediately after.

The final step is to switch from a real-time EFIT-based boundary control[29] to simple linear position estimators during the current quench.[30] The large vessel currents and rapidly evolving plasma equilibrium during the current quench can lead to inaccurate equilibrium reconstructions during that time, which in turn cause erroneous commands to be sent to the poloidal field coils. Linear combinations of a small number of magnetic diagnostic signals can provide estimates of the runaway beam centroid R & Z position even during very dynamic periods, avoiding gross control errors at the cost of losing fine boundary control.

The application of this simple control scheme proved effective in significantly increasing the lifetime of runaway electron beams in DIII-D [Fig. 4(b)] and reducing the

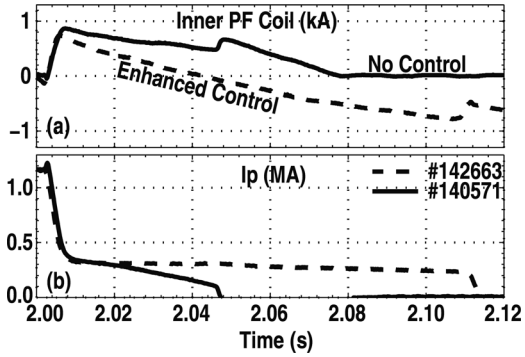

FIG. 4. Effects of control scenario on early runaway beam survival. Solid line indicates an uncontrolled case and dashed line indicates a case with enhanced controls implemented.

likelihood of fast runaway beam terminations near the current quench. However, it is important to note that stabilization of the runaway beam radial position becomes more difficult as the initial runaway current at the end of the current quench decreases. There is very little control over the dynamics of the initial runaway beam formation, so any control scheme can only improve the chances of avoiding excessive radial compression during the current quench, not guarantee that outcome. In this particular case, it is fortuitous for a high-current tokamak such as ITER that it will possess a very high runaway avalanche gain,[10] as that high gain will ensure the reliable production of large runaway electron fractions, without the large variation seen in DIII-D.

IV. CONTROL DURING PLATEAU PHASE

Once the initial survival of a runaway beam is assured, it can be sustained for arbitrary lengths of time through the application of I_p and position feedback control. An example of this control is provided in Fig. 5. A steady runaway electron current of 300 kA is held with I_p feedback control for over 0.6 s [Fig. 5(a)], terminating only when the ohmic solenoid reaches its flux limit and shuts down. This current control requires a loop voltage of over 4 V [Fig. 5(b)], providing an electric field of ~0.45 V/m. The large electric field is necessary because relativistic effects ensure that runaway electrons experience a finite drag from the surrounding plasma,[6] which in this case includes the background deuterium, carbon from the current quench, as well as residual argon from the injected argon pellet.[31] In addition, large angle scattering of the runaway electrons results in electron loss to the vessel wall, enhancing the effective resistance of the runaway current.[21,31,32]

During the current plateau, the HXR signal falls linearly by approximately 15% from its peak value [Fig. 5(c)]. This decrease in signal may be due to a dependence of the HXR detector sensitivity on the plasma position and geometry, or it may indicating a decline in the runaway population, despite the steady total current. Such a reduction in population can be explained by the relativistic nature of the runaway beam. For a relativistic electron beam, the velocity (v_{RE}) of each electron can be assumed to be approximately the speed of light, c, as at the energies in question (10's of MeV) a large fraction of the electron kinetic energy must be removed

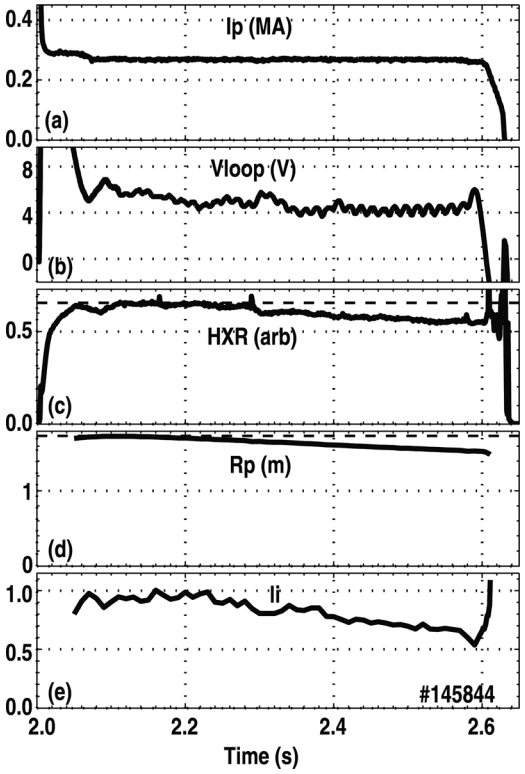

FIG. 5. Example of well controlled runaway beam position and current, sustained to the flux limit of the ohmic solenoid. Current quench (obscured) occurs at 2.0 s.

before v_{RE} drops appreciably below c. Therefore, using the high aspect ratio approximation, the total runaway beam current is given by

$$I_{RE} = eN_{RE}\frac{v_{RE}}{2\pi R_0} = eN_{RE}\frac{c}{2\pi R_0}, \tag{1}$$

where e is the electron charge, N_{RE} is the total number of runaway electrons, and R_0 is the runaway beam major radius. From Eq. (1), it is clear that

$$I_{RE} \propto \frac{N_{RE}}{R_0}. \tag{2}$$

As shown in Fig. 5(d), R_0 also declines gradually during the runaway current plateau by 13%. In order for I_{RE} to be held constant during this slow radial compression, it is necessary for N_{RE} to decline by a similar amount. This is consistent with the drop in HXR signal shown in Fig. 5(c).

The slow radial compression observed in Fig. 5(d) results from the inability of the DIII-D poloidal field coils to provide arbitrarily small vertical field for radial equilibrium. During the runaway plateau, the internal inductance (ℓ_i) of the runaway beam decreases steadily [Fig. 5(e)], similar to observations in Tore Supra.[22] This reduces the necessary B_z required to maintain a steady radial equilibrium. However, the poloidal field coil power supplies are unable to approach arbitrarily close to zero current, as they are single quadrant and operate at a finite duty factor. The power supplies typically reach a minimum current level early in the runaway plateau. Thus, B_z remains constant while ℓ_i decreases,

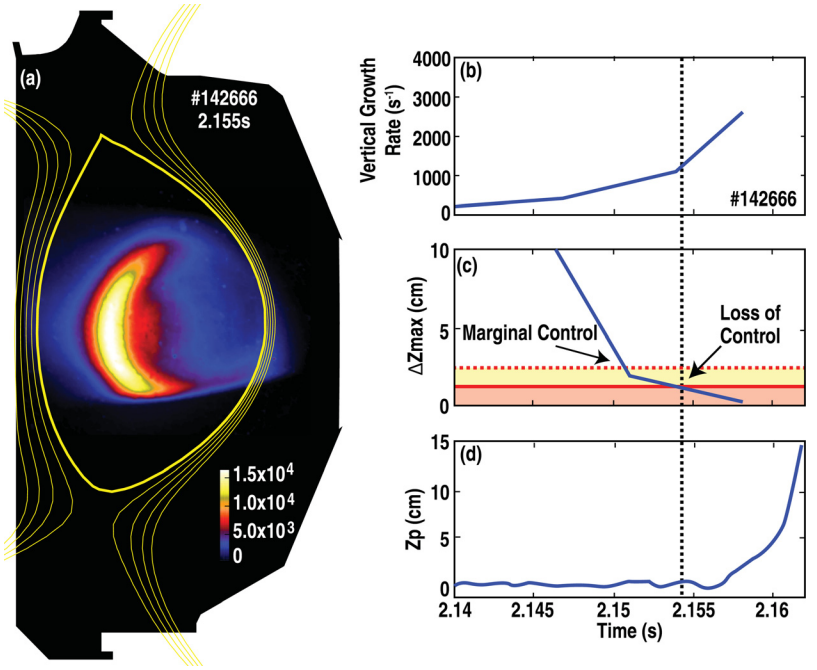

FIG. 6. Vertical controllability of an elongated runaway electron beam. (a) 2D image of visible synchrotron emission from runaway beam superimposed upon an outline of the DIII-D limiter boundary and the EFIT flux contours (plasma boundary indicated by thick line). (b) Vertical growth rate calculated using rigid plasma model. (c) Calculation of minimum controllable DZmax required. Marginal control area (light shading below dashed horizontal line) indicates when vertical control begins to saturate. Dark shaded area below solid horizontal line indicates where complete loss of vertical control occurs. (d) Runaway beam vertical position.

causing the runaway beam to be pushed slowly inward. Fortunately, this hardware-driven radial motion is slow enough that it does not pose a significant impediment to detailed runaway beam studies.

The empirical vertical stability properties of elongated, diverted runaway beams are consistent with standard vertical stability calculations. Although it is not a normal mode of operation, inner wall limited runaway beams have been elongated into a double null diverted (DND) shape. This configuration is vertically unstable, and requires active vertical stabilization from the DIII-D vertical control system. As shown in Fig. 6, vertical control is maintained until the runaway beam exceeds the pre-calculated controllability boundary of the vertical control system. The elongation and internal inductance of the DND runaway beam [Fig. 6(a)] rise gradually, causing the calculated vertical instability growth rate of the beam to increase as well [Fig. 6(b)]. The increasing growth rate reduces the maximum controllable vertical excursion (ΔZ_{max}) for the beam until the ΔZ_{max} capability falls below the pre-calculated minimum required ΔZ_{max} capability for the vertical control system [Fig. 6(c), minimum indicated by solid horizontal line].[33] The minimum required ΔZ_{max} is a function of power supply characteristics and system noise. The loss of vertical control is predicted to occur at that point (indicated by a dashed vertical line), and as expected, a vertical disruption event initiates soon thereafter [Fig. 6(d)]. This consistency between the predicted and empirical vertical stability boundaries indicates that position control of the runaway beam equilibrium does not differ substantially from that of more typical thermal plasmas.

V. INTERACTION WITH VESSEL WALL DURING PLATEAU PHASE

The runaway beam interaction with the inner wall displays a distinct threshold with respect to the minor radius of the runaway beam. This behavior is illustrated in Fig. 7. During the runaway current plateau [Fig. 7(a)], the runaway beam compresses slowly from a maximum minor radius of 0.45 m to approximately 0.3 m [Fig. 7(b)]. The indicators of the beam interaction with the vessel wall, including the required loop voltage to maintain the runaway current, the HXR emission, and carbon line emission remain fairly

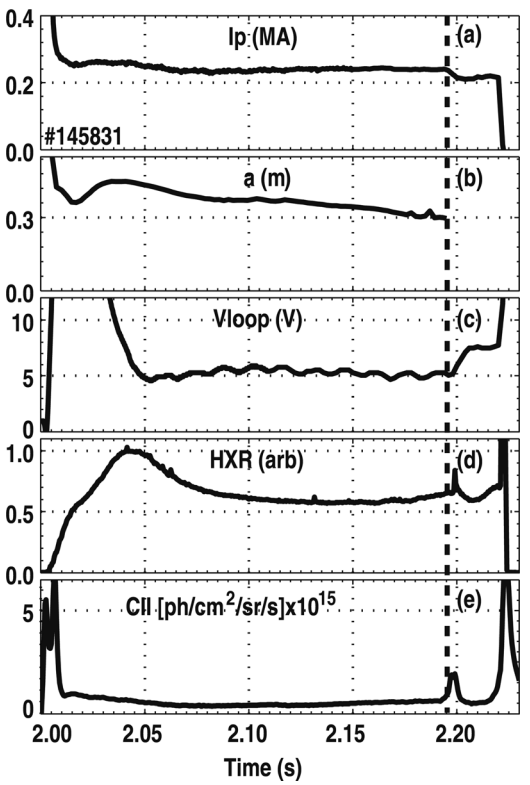

FIG. 7. Appearance of enhanced wall interaction during a slow radial compression. The dashed vertical line indicates the time at which the threshold is crossed. EFIT fails at that point, so no further minor radius data is available in (b).

constant [Figures 7(c)–7(e)] during this time. However, once the runaway beam compresses to a minor radius of 0.3 m (indicated by the dashed vertical line in Fig. 7), a threshold is crossed and the nature of the beam interaction with the wall changes distinctly. At this that time, I_p falls and the loop voltage (V_{loop}) jumps rapidly in an unsuccessful attempt to maintain I_p. This jump in the loop voltage required to sustain the runaway current is indicative of either increased runaway deconfinement to the wall, increased drag from wall impurities, or both. The increased level of deconfinement is supported by the onset of short HXR spikes, indicating runaway losses to the wall, in Fig. 7(d). Likewise, a bloom of carbon from the graphite wall tiles is evident in Fig. 7(e), indicating increased impurity levels in the runaway beam. This period of enhanced inner wall interaction is quickly followed by the termination of the runaway beam.

The onset of this enhanced inner wall interaction corresponds to the core of the runaway beam's synchrotron emission impacting the vessel wall. Figure 8 displays the I_p and minor radius traces from Fig. 7, as well as images of the visible synchrotron emission at various times (2.05, 2.10, and 2.190 s) during the runaway plateau. The synchrotron emission images are overlaid on an outline of the DIII-D first wall and the EFIT boundary for clarity. During the quiescent period of the runaway plateau (images at 2.05 and 2.10 s), the bright core of the runaway beam's synchrotron emission maintains a gap of a few 10 s of cm from the inner wall, even though the flux boundary is limited on the wall. The synchrotron core continues to move toward the inner wall as the beams minor radius decreases, until it finally impacts the wall at 2.190 s, coincident with the onset of the enhanced wall interaction.

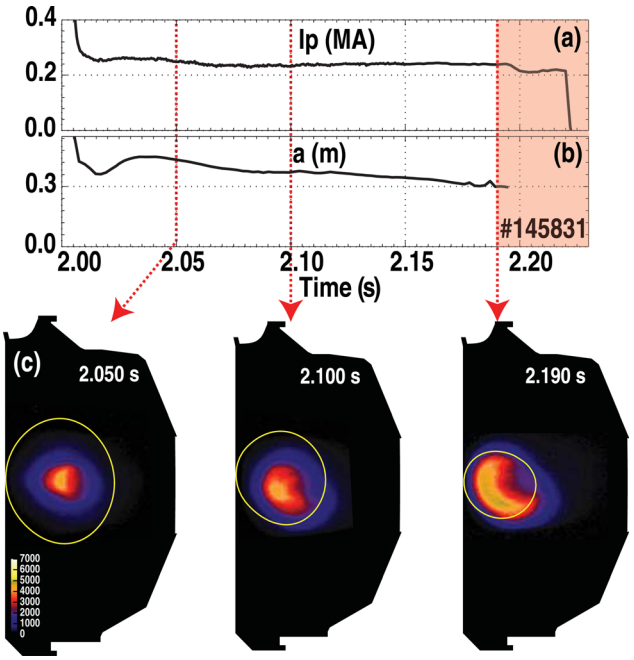

FIG. 8. Correspondence of synchrotron core impacting inner wall and onset of enhanced wall interaction. The images depict the EFIT boundary (solid line) and a 2D image of runaway beam's visible synchrotron emission superimposed over an outline of DIII-D limiter structure (black background). The shaded zones in plots (a) and (b) indicate when the enhanced wall interaction is occurring.

It is not clear if the bright core of the synchrotron emission corresponds to a peak in runaway current density, energy, or both. Peaking of the runaway current density would increase the amplitude of the entire visible synchrotron continuum near the location of the peak, creating a high-intensity core like that observed in the images. However, peaking of the runaway electron energy at the same location would shift the visible synchrotron distribution toward lower wavelengths, producing the same result. The camera images alone cannot separate these effects.

The enhanced inner wall interaction threshold occurs within a narrow range of radii over a wide range of runaway current trajectories. Figure 9 displays the trajectories of runaway electron discharges in a phase space of I_p and minor radius, starting from the end of the current quench (denoted by filled triangles) and ending at the V_{loop} inflection (filled circles), which is typically the first and most reliable indication of enhanced wall interaction. The dataset is comprised of those controlled, limited runaway plateaus that terminated early, before the ohmic flux limit was reached. Figure 9 shows that regardless of whether I_p was ramped down (e.g., solid red line) or the runaway beam compressed at a constant I_p (dashed red line), the V_{loop} inflection occurs within a narrow range of minor radii, approximately 0.30-0.35 m. This range holds over an almost 3× variation in runaway current at the time of the V_{loop} inflection. The edge safety factor q_{edge} exceeds 4 in all cases, and is much higher in the ramp-down cases. The consistency of the minor radius threshold over a wide range of current trajectories and q_{edge} values supports the evidence from the synchrotron emission images that the onset of the enhanced inner wall interaction is determined by the proximity of the runaway synchrotron core to the inner wall rather than MHD considerations.

The onset of enhanced wall interaction is a common precursor to, but not immediate cause of, the final runaway electron beam termination. For the discharges of Fig. 9, the timespan between the loop voltage jump and the final fast termination varies by more than a factor of four (30-125 ms). Typically, the MHD activity that terminates the runaway

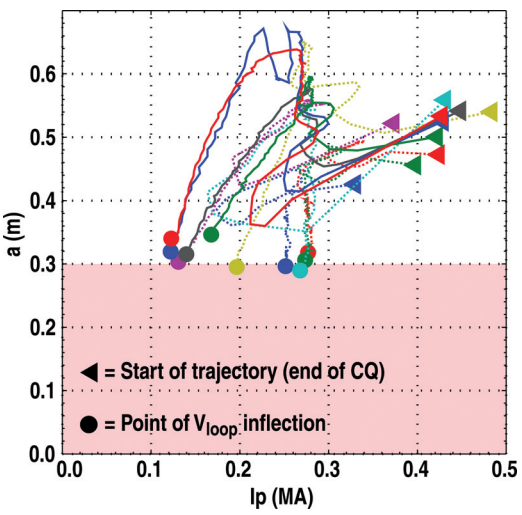

FIG. 9. Runaway beam trajectories in I_p and minor radius from current quench (solid triangles) until V_{loop} inflection (solid circles).

beam manifests as a non-rotating $n = 1$ mode, as detected by magnetic saddle loops and the BGO scintillator array.[34]

Unlike the inner wall interaction, the runaway beam interaction with the outer limiter exhibits a threshold when the core of the runaway synchrotron emission is still far from the outer limiter. An example is shown in Fig. 10. In this case, the plasma is allowed to drift outward, switching from limiting on the inner wall to limiting on the outer graphite bumper limiters[1] around 2.140 s. The runaway current is held at a steady level (280 kA) until an enhanced wall interaction event causes it to drop suddenly at 2.183 s [Fig. 10(a)]. This event is also evident in the sudden change in HXR signal at the same time [Fig. 10(b)]. However, at this time the synchrotron emission core is still tens of centimeters from the outer limiters [Fig. 10(c)], in stark contrast to the inner wall threshold.

A possible explanation for the longer distance interaction with the outboard limiter compared to the inner wall is the outward shift of the runaway electron drift orbits from the magnetic flux surfaces. The magnitude of this drift is given by[35]

$$\Delta R_{RE} = \frac{\bar{q} \mathrm{W}_{RE}}{ecB}, \tag{3}$$

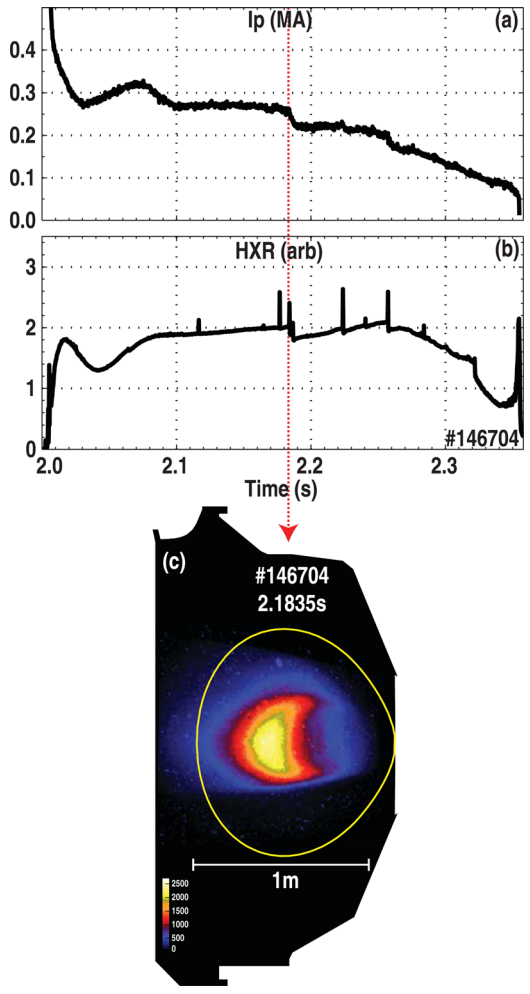

FIG. 10. Example of long-distance runaway beam interaction with outer limiter.

where ΔR_{RE} is the outward shift, $\bar{q}$ is the drift-averaged safety factor, W_{RE} is the electron energy, and B is the applied toroidal field. The outward shift for case shown in Fig. 10 can be estimated using a few reasonable assumptions. Assuming $\bar{q} = 8$ (mean value of the EFIT calculated q profile), $\mathrm{W}_{RE} = 20$ MeV (peak runaway electron energies as high as 35–40 MeV have been observed), and B = 2T gives $\Delta R_{RE} \sim 0.25$ m. Note that the most energetic electrons (e.g., those exceeding 20 MeV) will possess proportionally larger outward shifts. The calculated shift is of the same scale length as the gap observed between the synchrotron emission core and the outer limiter at the time of the observed interaction event, making runaway electron drift orbits a viable explanation for this long-distance interaction.

Collecting together the data from the enhanced wall interaction threshold events discussed above, a region for safely positioning the runaway beam with minimal wall interaction emerges. At the bottom of Fig. 11, the radial distribution of the inner wall threshold, collected from ten separate events, is plotted and shaded, indicating the minimum safe radius for the runaway beam. Likewise, a region is shaded at the top to denote the outer limiter threshold from three observed events. Between these inner and outer limits exists a zone (no shading) of minimal wall interaction. Plotted within that zone is the full extent of the radial motion of the five controlled runaway beams that survived to the ohmic flux limit without any observed enhanced wall interaction. The existence of these quiescent runaway beams provides positive evidence that a safe position exists to hold runaway beams for long time-scales with minimal wall interaction.

VI. CONTROLLED DISSIPATION OF RUNAWAY ELECTRON BEAM

Once a runaway electron beam has been moved to a safe position, its total energy can be gradually dissipated to mitigate the threat it poses to the vessel. This is accomplished by a controlled ramp-down of the runaway current, as shown in Fig. 12. The runaway electron current [Fig. 12(a), solid line] closely follows the prescribed target (dashed line). Well-controlled ramp-downs from 300 kA down to 65 kA have been demonstrated. The HXR signal [Fig. 12(b)] falls with

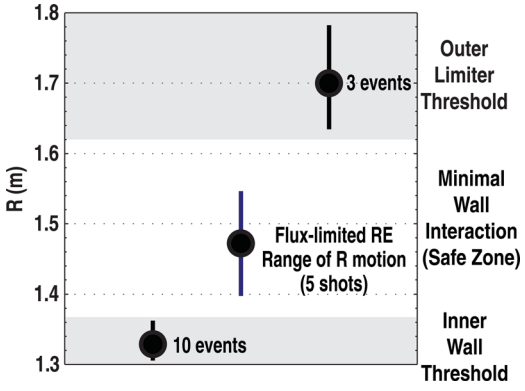

FIG. 11. "Safe Zone" for radial positioning of runaway beam with minimal wall interaction. The solid circles indicate the mean of each dataset, and the vertical lines the full radial extent. Shaded regions indicate "danger zones" for positioning the runaway beam that result in an enhanced wall interaction threshold being crossed.

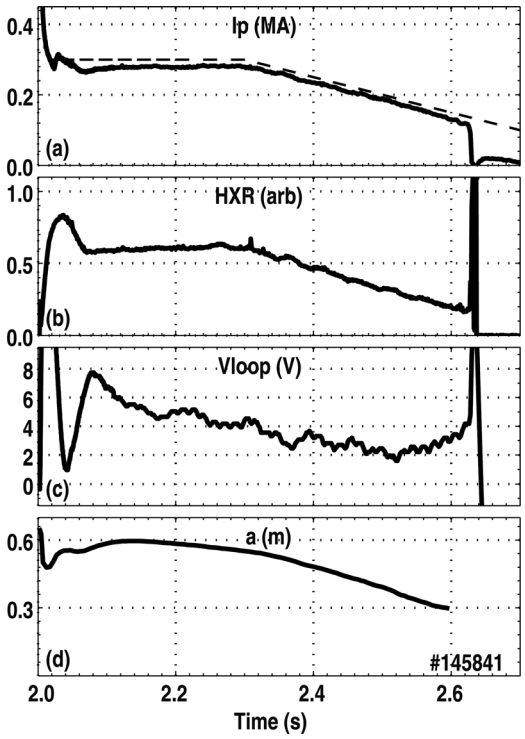

FIG. 12. Example of controlled runaway beam ramp-down. Dashed line in (a) indicates control target. EFIT minor radius data is not available in (d) after the enhanced wall interaction threshold is crossed at 2.6 s.

the runaway current, indicating a declining runaway electron population, as desired. The rate of change of the HXR signal is faster than that of the plasma current because the runaway beam is slowly compressing during the ramp-down, as discussed in Sec. IV. The runaway current is still being sustained by a positive loop voltage [Fig. 12(c)], as the controlled ramp-down is slower than the natural dissipation caused by large-angle scattering losses to the wall and drag with the background plasma. The applied electric field is replacing runaway electron at a slower rate than they are lost, resulting in a gradual decline in runaway population. For the present case, the runaway beam eventually suffers a fast termination after hitting the 0.3 m minor radius inner wall interaction threshold [Fig. 12(d)]. As noted in Sec. IV, this is due to the inability of the poloidal field power supplies to approach arbitrarily close to 0 A in order to maintain a consistent equilibrium during the ramp-down. With appropriate power supplies, there is no intrinsic barrier to accomplishing a full controlled runaway current ramp-down.

An illustrative example of a full ramp-down under less carefully controlled conditions is presented in Fig. 13. After a brief runaway plateau period, a large negative loop voltage is applied with no I_p control [Fig. 13(a)]. This drives down the runaway electron current at a rapid rate of -3 MA/s [Fig. 13(b)]. In contrast to the ramp-down case of Fig. 12, no replacement of lost runaway electrons is occurring. A unique feature of this ramp-down is that it does not experience a clear inner wall interaction threshold at $a = 0.3$ m [Fig. 13(c), left dashed vertical line], and is able to compress to $a = 0.24$ m before a clear inflection in I_p is observed. This new behavior is likely due to the synchrotron emission core being positioned near the outer edge of the beams magnetic boundary at the $a = 0.3$ m point, as shown in Fig. 13(f). The outward shift may be a result of either the fast ramp-down or a coil configuration that had a pair of inner poloidal field coils pushing outward on the runaway beam, both of which were unique to this discharge. By the time the beam does experience clear signs of enhanced wall interaction (right dashed vertical line), the effects are small, resulting in neither a complete loss of runaway current signal nor neutron signal [Fig. 13(d)]. Instead, the beam recovers and proceeds to ramp down fully. There are fast deconfinement events evident in the neutron signal near the very end of the ramp-down, but the fast

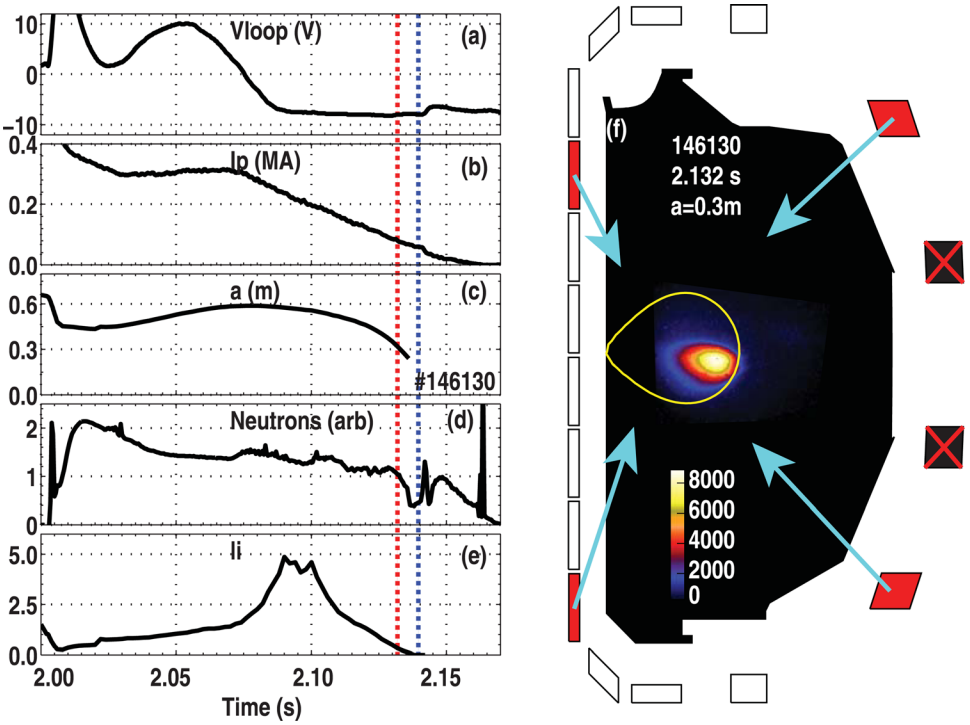

FIG. 13. Example of full runaway beam ramp-down. Large negative loop voltage (a) produces a rapid ramp-down in I_p (b), and corresponding reduction in minor radius (c). Left dashed vertical line indicates where $a = 0.3$ m, which is the time slice shown in (f). Right dashed vertical line indicates the clear onset of enhanced wall interaction at $a = 0.24$ m. (d) Photo-neutron signal and (e) EFIT ℓ_i. Arrows in (f) indicate the direction in which the coils are pushing the runaway beam.

spikes change the baseline of the declining neutron signal very little, indicating that there is only a small portion of the runaway electron population (and energy) lost in those events.

Although it provides an example of a complete runaway current ramp-down, this particular scenario is not appropriate for elongated, vertically unstable runaway beams. The strong negative loop voltage causes ℓ_i to rise rapidly [Fig. 13(e)], so that vertical stabilization would likely fail and result in an undesirable vertical displacement event. Slower runaway current ramp rates, as illustrated in Fig. 12, provide conditions more conducive for maintaining active vertical control.

VII. CONCLUSIONS

Control techniques have been developed in the DIII-D tokamak to stabilize and maintain both the vertical and radial positions of post-disruption runaway electron beams and then dissipate their energy in a gradual, controlled manner. During and immediately after the current quench, excessive radial compression is avoided by a combination of techniques, improving the likelihood of runaway beams surviving this dynamic period without a fast termination. Once stabilized, the runaway beams are held in a steady state (out to the ohmic flux limit) with the application of active plasma current and position controls. Beam interaction with the vessel wall can be minimized by avoiding distinct thresholds for enhanced wall interaction at small and large radii, corresponding to inner wall and outer limiter interaction. Staying within the "safe zone" between those radial thresholds allows for the sustainment of long-lived, quiescent runaway beams. The total beam energy and runaway electron population can then be dissipated slowly by a ramp-down of the runaway current.

ACKNOWLEDGMENTS

This research was supported by the U.S. Department of Energy under Contract Nos. DE-FC02-04ER54698, DE-AC05-00OR22725, and DE-FG02-07ER54917.

[1]J. L. Luxon, Nucl. Fusion **42**, 614 (2002).
[2]F. C. Shüller, Plasma Phys. Controlled Fusion **37**, A135 (1995).
[3]H. Dreicer, Phys. Rev. **115**, 238 (1959).
[4]H. M. Smith and E. Verwichte, Phys. Plasmas **15**, 072502 (2008).
[5]P. Helander, L. G. Eriksson, and F. Andersson, Plasma Phys. Controlled Fusion **44**, B247 (2002).
[6]J. W. Connor and R. J. Hastie, Nucl. Fusion **15**, 415 (1975).
[7]V. Sizyuk and A. Hassanein, Nucl. Fusion **49**, 095003 (2009).
[8]M. N. Rosenbluth and S. V. Putvinski, Nucl. Fusion **37**, 1355 (1997).
[9]ITER Physics Basis Editors *et al.*, Nucl. Fusion **39**, 2137 (1999).
[10]T. C. Hender, J. C. Wesley *et al.*, Nucl. Fusion **47**, S128–S202 (2007).
[11]R. D. Gill, Nucl. Fusion **33**, 1613 (1993).
[12]R. D. Gill, Nucl. Fusion **40**, 163 (2000).
[13]R. D. Gill, Nucl. Fusion **42**, 1039 (2002).
[14]V. V. Plyusnin, V. Riccardo, R. Jaspers, B. Alper, V. G. Kiptily, J. Mlynar, S. Popovichev, E. de La Luna, F. Andersson, and JET EFDA contributors, Nucl. Fusion **46**, 277 (2006).
[15]M. Lehnen, S. S. Abdullaev, G. Arnoux, S. A. Bozhenkov, M. W. Jakubowski, R. Jaspers, V. V. Plyusnin, V. Riccardo, and U. Samm, J. Nucl. Mater. **390–391**, 740 (2009).
[16]R. Yoshino, Y. Neyatani, N. Hosogane, S. W. Wolfe, M. Matsukawa, and H. Ninomiya, Nucl. Fusion **33**, 1599 (1993).
[17]R. Yoshino, S. Tokuda, and Y. Kawano, Nucl. Fusion **39**, 151 (1999).
[18]R. Yoshino and S. Tokuda, Nucl. Fusion **40**, 1293 (2000).
[19]F. Saint-Laurent, G. Martin, J. Bucalossi, F. Sourd, and L. G. Eriksson, in *32nd EPS Conference on Plasma Physics* (Tarragona, Spain, 2005) Vol. 29C, P-2.064, http://eps2005.ciemat.es/papers/pdf/P2_064.pdf.
[20]F. Saint-Laurent, C. Reux, J. Bucalossi, A. Loarte, S. Bremond, C. Gil, P. Moreau, and J. L. Ségui, in *Proceedings of the 36th EPS Conference on Plasma Physics* (Sophia, Bulgaria, 2009) Vol. 33E, P-4.205, http://epsppd.epfl.ch/Sofia/pdf/P4_205.pdf.
[21]F. Saint-Laurent, C. Reux, J. Bucalossi, A. Loarte, S. Bremond, C. Gil, P. Maget, P. Moreau, and J. L. Ségui, in *Proceedings of the 23rd IAEA Fusion Energy Conference* (Daejon, Korea, 2010) EXS/P2-16, http://www-pub.iaea.org/MTCD/Meetings/PDFplus/2010/cn180/cn180_papers/exs_p2-16.pdf.
[22]F. Saint-Laurent, J. Bucalossi, C. Reux, S. Bremond, D. Douai, C. Gil, and P. Moreau, in *Proceedings of 38th EPS Conference on Plasma Physics* (Strasbourg France, 2011), Vol. 35G, O3.118, http://ocs.ciemat.es/EPS2011PAP/pdf/O3.118.pdf.
[23]T. Fülöp, H. M. Smith, and G. Pokol, Phys. Plasmas **16**, 022502 (2009).
[24]V. A. Izzo, E. M. Hollmann, A. N. James, J. H. Yu, D. A. Humphreys, L. L. Lao, P. B. Parks, P. E. Sieck, J. C. Wesley, R. S. Granetz, G. M. Olynyk, and D. G. Whyte, Nucl. Fusion **51**, 063032 (2011).
[25]T. E. Evans, P. L. Taylor, A. G. Kellman, P. B. Parks, D. A. Humphreys, R. L. Lee, M. J. Schaffer, J. A. Leuer, A. W. Hyatt, D. G. Whyte, S. C. Luckhardt, D. Gray, J. Zhang, R. W. Harvey, T. C. Jernigan, L. R. Baylor, in *Proceedings of the 17th IAEA Fusion Energy Conference* (Yokohama, Japan, 1998), Vol. 3, pp. 847–850.
[26]E. M. Hollmann, T. C. Jernigan, P. B. Parks, A. Boedo, T. E. Evans, M. Groth, D. A. Humphreys, A. N. James, M. J. Lanctot, D. Nishijima, D. L. Rudakov, H. A. Scott, E. J. Strait, M. A. Van Zeeland, J. C. Wesley, W. P. West, W. Wu, and J. H. Yu, Nucl. Fusion **48**, 115007 (2008).
[27]W. W. Heidbrink, Rev. Sci. Instrum. **57**, 1769 (1986).
[28]A. N. James, E. M. Hollmann, and G. R. Tynan, Rev. Sci. Instrum. **81**, 10E306 (2010).
[29]J. R. Ferron, M. L. Walker, L. L. Lao, H. E. St. John, D. A. Humphreys, and J. A. Leuer, Nucl. Fusion **38**, 1055 (1998).
[30]J. A. Leuer, B. J. Xiao, D. A. Humphreys, M. L. Walker, A. W. Hyatt, G. L. Jackson, D. Mueller, B. G. Penaflor, D. A. Piglowski, R. D. Johnson, A. S. Welander, Q. P. Yuan, H. Z. Wang, J. R. Luo, and EAST Team, Fusion Sci. Technol. **57**, 48 (2010).
[31]E. M. Hollmann, P. B. Parks, D. A. Humphreys, N. H. Brooks, N. Commaux, N. Eidietis, T. E. Evans, R. Isler, A. N. James, T. C. Jernigan, J. Munoz, E. J. Strait, C. Tsui, J. Wesley, and J. H. Yu, Nucl. Fusion **51**, 103026 (2011).
[32]C. Amsler *et al.*, Phys. Lett. B **667**, 261 (2008).
[33]D. A. Humphreys, T. A. Casper, N. Eidietis, M. Ferrara, D. A. Gates, I. H. Hutchinson, G. L. Jackson, E. Kolemen, J. A. Leuer, J. Lister, L. L. LoDestro, W. H. Meyer, L. D. Pearlstein, A. Portone, F. Sartori, M. L. Walker, A. S. Welander, and S. M. Wolfe, Nucl. Fusion **49**, 115003 (2009).
[34]A. N. James, M. E. Austin, N. Commaux, N. W. Eidietis, T. E. Evans, E. M. Hollmann, D. A. Humphreys, A. W. Hyatt, V. A. Izzo, T. C. Jernigan, R. J. La Haye, P. B. Parks, E. J. Strait, G. R. Tynan, J. C. Wesley, and J. H. Yu, Nucl. Fusion **52**, 013007 (2011).
[35]X. Guan, H. Qin, and N. J. Fisch, Phys. Plasmas **17**, 092502 (2010).